Importance of water mass formation regions for the air-sea CO2 flux estimate in the Southern Ocean

Leticia Barbero, Jacqueline Boutin, Liliane Merlivat, Nicolas Martin, Taro Takahashi, Stewart C. Sutherland, Rik H. Wanninkhof

Importance of water mass formation regions for the air-sea CO_2 flux estimate in the Southern Ocean

Leticia Barbero,[1] Jacqueline Boutin,[1] Liliane Merlivat,[1] Nicolas Martin,[1] Taro Takahashi,[2] Stewart C. Sutherland,[2] and Rik Wanninkhof[3]

Received 5 March 2010; revised 12 August 2010; accepted 24 September 2010; published 1 February 2011.

[1] CARIOCA drifters and ship data from several cruises in the Subantarctic Zone (SAZ) of the Pacific Ocean, approximately 40°S–55°S, have been used in order to investigate surface CO_2 partial pressure (pCO_2) and dissolved inorganic carbon (DIC) patterns. The highest DIC values were determined in regions of deep water formation, characterized by deep mixed layer depths (MLD) as estimated from Argo float profiles. As a result, these areas act as sources of CO_2 to the atmosphere. Using an empirical linear relationship between DIC, sea surface temperature (SST), and MLD, we then combine DIC with A_T based on salinity and compute pCO_2. Finally, we derive monthly fields of air-sea CO_2 flux in the SAZ. Our fit predicts the existence of a realistic seasonal cycle, close to equilibrium with the atmosphere in winter and a sink when biological activity takes place. It also reproduces the impact that deep water formation regions close to the Subantarctic Front (SAF) and in the eastern part of the SAZ have on the uptake capacity of the area. These areas, undersampled in previous studies, have high pCO_2, and as a result, our estimates (0.05 ± 0.03 PgC yr^{-1}) indicate that the Pacific SAZ acts as a weaker sink of CO_2 than suggested by previous studies which neglect these source regions.

Citation: Barbero, L., J. Boutin, L. Merlivat, N. Martin, T. Takahashi, S. C. Sutherland, and R. Wanninkhof (2011), Importance of water mass formation regions for the air-sea CO_2 flux estimate in the Southern Ocean, *Global Biogeochem. Cycles*, *25*, GB1005, doi:10.1029/2010GB003818.

1. Introduction

[2] As a result of the burning of fossil fuels and deforestation, atmospheric levels of carbon dioxide, CO_2, are rapidly increasing [*Keeling et al.*, 1995; *Denman et al.*, 2007]. Almost one fourth of these CO_2 emissions are absorbed by the ocean [*Sabine et al.*, 2004; *Canadell et al.*, 2007; *Le Quéré et al.*, 2010]. According to the fourth assessment IPCC report on climate change [*IPCC*, 2007] the current global oceanic uptake is 2.2 ± 0.5 PgC yr^{-1}. However, there are uncertainties concerning the large scale integrated CO_2 flux figures and, in particular, estimates in the Southern Ocean disagree [*Denman et al.*, 2007; *Gruber et al.*, 2009]. Due to the scarcity of observations in the southern Pacific Ocean, the largest oceanic basin in the Southern Hemisphere, the air-sea CO_2 flux in this region is still poorly known.

[3] The Southern Ocean (south of about 30°S) is a sink area for atmospheric CO_2, in atmospheric or ocean inversion models [*Friedlingstein et al.*, 2006; *Gruber et al.*, 2009] as well as in data-based approaches [*Metzl et al.*, 1999; *Takahashi et al.*, 2002, 2009a]. However, this is the oceanic region where the largest discrepancies concerning the actual magnitude of the flux exist (see, e.g., *Gruber et al.* [2009] for the area south of 44°S). Direct comparisons are complicated because different authors define the Southern Ocean differently. Estimations based on pCO_2 measurements have pointed in general toward a large sink in the Subantarctic Zone (SAZ) of the Southern Ocean ranging from 0.8 PgC yr^{-1} to 1.1 PgC yr^{-1} [*Metzl et al.*, 1999; *McNeil et al.*, 2007; *Boutin et al.*, 2008]. Ocean inversion flux studies suggest smaller sinks, closer to 0.3 PgC yr^{-1} for the area south of 44°S [*Gruber et al.*, 2009]. These authors found up to a twofold difference between ocean inversion models, atmospheric inversions and direct estimations in the Southern Ocean.

[4] Within the Southern Ocean, because the southern Pacific is the largest basin, this is potentially the largest contributor to the CO_2 sink. It is therefore of great importance to better constrain fluxes in this region if we want to improve flux estimations in all the Southern Ocean.

[5] The southern Pacific Ocean south of about 40°S is characterized by the presence of very deep mixed layers in late winter, in particular close to the Subantarctic Front (SAF) and the western coast of South America [*de Boyer Montégut et al.*, 2004; *Dong et al.*, 2008]. These are areas of formation of Subantarctic Mode Water (SAMW) and

[1]Laboratoire d'Océanographie et du Climat: Expérimentations et approches numériques, IPSL, CNRS, IRD, UPMC, Paris, France.
[2]Lamont-Doherty Earth Observatory, Columbia University, Palisades, New York, USA.
[3]Atlantic Oceanographic and Meteorological Laboratory, NOAA, Miami, Florida, USA.

0886-6236/11/2010GB003818

Antarctic Intermediate Water (AAIW), and hydrographic properties are nearly homogeneous in the eastern part of the southern Pacific Ocean [*McCartney*, 1977; *Tsuchiya and Talley*, 1998; *Hanawa and Talley*, 2001; *Saenko et al.*, 2003]. The southern Pacific Ocean is also one of the least sampled regions of the global ocean, particularly in the winter and in the eastern part of the basin [*Leth et al.*, 2004; *Takahashi et al.*, 2009a]. Our study provides new insights into the CO_2 fluxes of this poorly known region.

[6] In this paper, we present a new approach to estimate the air-sea CO_2 flux in the southern Pacific Ocean based on the combination of data from underway surface ship measurements and autonomous CARIOCA drifters, along with data from ARGO profiles, an associated mixed layer depth (MLD) climatology from *Dong et al.* [2008] for the Southern Ocean and ocean-color satellite images. Our data includes surface measurements throughout the year including the austral winter.

[7] In the following sections we first present the data and the methodology used. We then describe the variability observed on basin-wide scale, and the relationship observed between CO_2 parameters, MLD and temperature. We also explore the possibility of introducing chlorophyll concentration derived from satellite images as an additional variable in our parameterization. The following section concerns the creation of monthly maps of CO_2 parameters and air-sea CO_2 fluxes. The final sections deal with a comparison with previous estimates, a look into interannual variability and our final conclusions.

2. Data and Methodology

[8] A least squares approach has been applied to surface CO_2 data from the southern Pacific Ocean to derive a fit between the parameters of the carbon dioxide system and physical parameters in the area. We use a large data set compiled from surface measurements by autonomous CARIOCA drifters and ship cruises in the SAZ of the Pacific Ocean. The database has been split into two sets: the first set includes the data from the CARIOCA buoys (yearlong measurements including winter data) and four Palmer cruises (Figure 1a), and has been used for establishing the fit. The second group of independent data is composed of data from 3 additional Palmer cruises, WOCE cruises and additional campaigns (Figure 1e and Table 1) and has been used to evaluate the validity of the fit in terms of DIC and pCO_2.

2.1. Carioca pCO_2 Measurements

[9] Two CARIOCA drifters deployed in 2004 in the western part of the SAZ of the Pacific Ocean drifted eastward for more than 1 year [*Boutin et al.*, 2008]. Their trajectories are shown on Figure 1a. These drifters measured pCO_2, sea surface temperature (SST), salinity (SSS) and fluorescence (only one of them) at 2-m depth, as well as surface wind speed, U, atmospheric pressure, Pa, and air temperature at hourly intervals at a height of 2 m [*Boutin et al.*, 2008]. The pCO_2 is analyzed by measuring the change in the optical absorbance of a pH sensitive dye diluted in a constant alkalinity seawater at three different wavelengths. This ensures an internal control of the calibration of the CO_2 as is described in detail by *Copin-Montegut et al.* [2004]. The accuracy of the pCO_2 is of about 3 μatm based on laboratory calibration and CARIOCA-ship intercomparisons [*Bates et al.*, 2000; *Hood and Merlivat*, 2001; *Copin-Montegut et al.*, 2004]. Data were transmitted in real time via ARGOS. The buoys were active from April 2004 to April and June 2005, respectively (Figure 1b and Table 1).

2.2. Ship pCO_2 Measurements

[10] For our fit, we have used surface data from four cruises carried out by the RVIB Palmer from 2004 to 2006 in the southern Pacific Ocean (Figure 1a). Measurements include pCO_2, SST and SSS. Only data within the SAZ have been considered. In this work we use the same definition for the SAZ as *Boutin et al.* [2008], i.e., the area comprised between the Subantarctic Front (SAF) and the Subtropical Front (STF). In the Pacific Ocean the SAZ is located approximately between 40°S and 55°S. Validation of pCO_2 estimated from the DIC fit has been carried out using underway pCO_2 measurements from cruises between 1979 and 2008 (Figure 1e and Table 1).

[11] Continuous underway pCO_2 measurements were carried out onboard the RVIB Palmer using a Licor non-dispersive infrared CO_2 gas analyzer system coupled with a shower-type gas-water equilibrator described by *Newberger* [2004]. The analyzer was calibrated hourly using five reference gas mixtures certified by NOAA/ESRL ranging from 100 ppm to 800 ppm mole fraction CO_2 in dry air. The data are listed at the LDEO web site (http://www.ldeo.columbia.edu/res/pi/CO2/carbondioxide/pages/pCO2data.html).

2.3. Estimation of Total Alkalinity

[12] Total alkalinity, A_T, was computed from SST and SSS using the alkalinity-temperature-salinity relationship proposed by *Lee et al.* [2006] for the Southern Ocean:

$$A_T = 2305 + 52.48 \cdot (SSS - 35) + 2.85 \cdot (SSS - 35)^2 - 0.49 \cdot (SST - 20) + 0.086 \cdot (SST - 20)^2 \quad (1)$$

[13] The validity of this relationship in the area was checked by comparing A_T estimated using it with actual

Figure 1. (a) Trajectories followed by the CARIOCA drifters (red for 01110, blue for 03740) and Palmer cruises (brown for 0403, yellow for 051B, green for 0507 and purple for 067A). The buoys and cruises went from west to east. The dotted line represents the location of the STF, the black line shows the location of the SAF. The *x* axis is longitude, and the *y* axis is latitude. (b) Same trajectories color coded for month, showing available data depending on month of the year. (c) Surface pCO_2 (μatm) along the trajectories. (d) Calculated DIC (μmol kg^{-1}) along the trajectories, black dots indicate position of colocated ARGO float profiles. (e) Trajectories of the cruises used for validation of DIC and pCO_2.

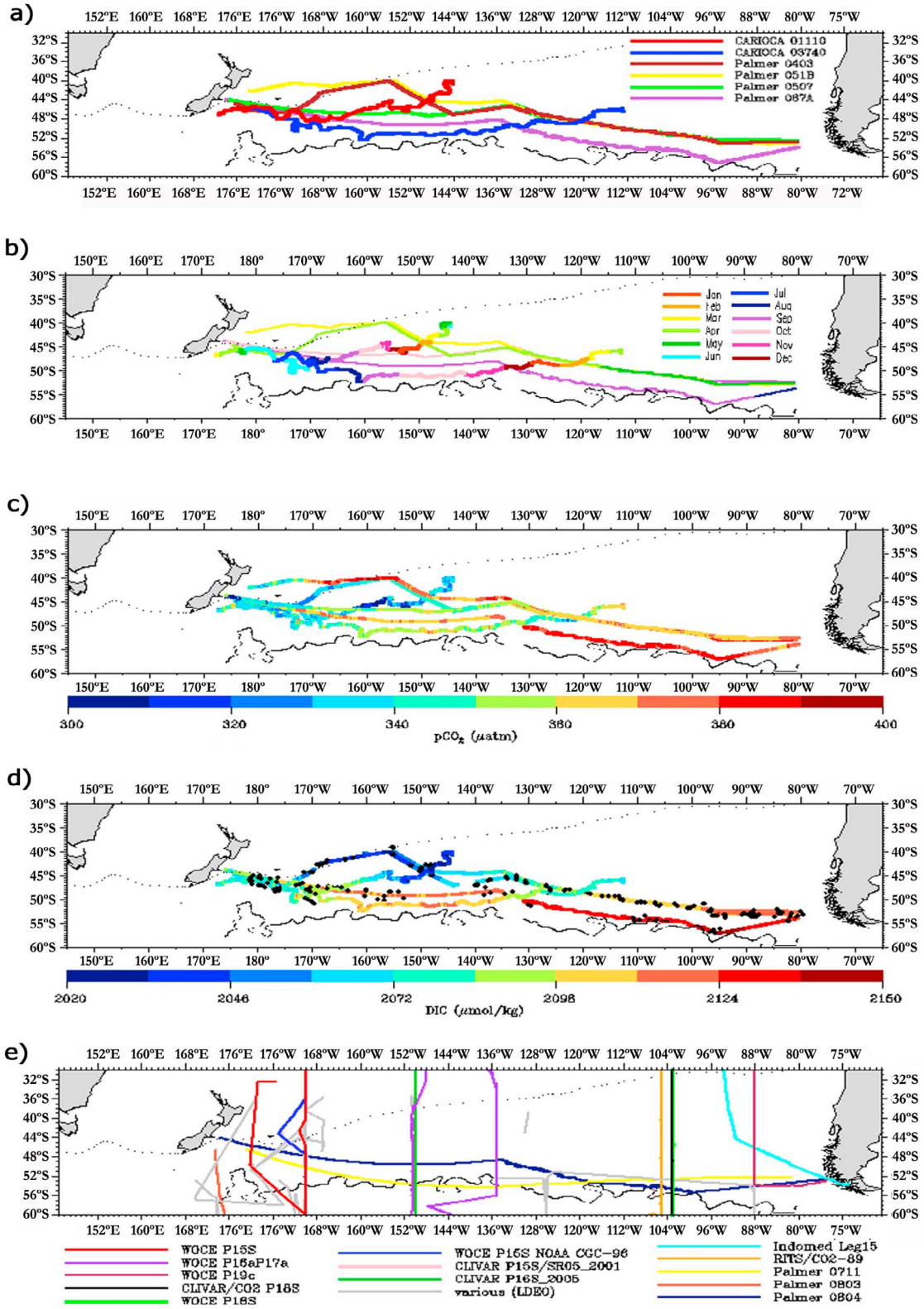
a)
CARIOCA 01110
CARIOCA 03740
Palmer 0403
Palmer 051B
Palmer 0507
Palmer 087A
b)
Jan
Feb
Mar
Apr
May
Jun
Jul
Aug
Sep
Oct
Nov
Dec
c)
300
320
340
360
380
400
pCO2 (µatm)
d)
2020
2046
2072
2098
2124
2150
DIC (µmol/kg)
e)
WOCE P15S
WOCE P16aP17a
WOCE P19c
CLIVAR/CO2 P18S
WOCE P18S
WOCE P15S NOAA CGC-96
CLIVAR P15S/SR05_2001
CLIVAR P16S_2005
various (LDEO)
Indomed Leg15
RITS/CO2-89
Palmer 0711
Palmer 0803
Palmer 0804

Figure 1

Table 1. Dates and Location of Valid Measurements for the Two CARIOCA Buoys (01110 and 03740) and the Four Ship Cruises Used in the Study (Palmer 0403, 051B, 0507, and 067A [*Takahashi et al.*, 2009b]), Plus Details for the Validation Cruises Used

Year	Buoy/Cruise	Start of pCO_2 Measurements	End of pCO_2 Measurements	Starting Position	Final Position
		Data Used for the Computation of the Empirical DIC Relationship			
2004	Buoy 01110	29/03/04	11/06/05	46.8°S 172.7°E	40.8°S 215.9°E
2004	Buoy 03740	12/04/04	20/04/05	46.3°S 177.7°E	46.3°S 247.3°E
2004	Palmer 0403	16/04/04	08/05/04	44.7°S 175.7°E	52.3°S 279.3°E
2005	Palmer 051B	08/03/05	21/03/05	42.2°S 178.4°E	52.9°S 279.2°E
2005	Palmer 0507	25/09/05	20/10/05	52.5°S 279.4°E	44.0°S 174.8°E
2006	Palmer 067A	30/08/06	22/09/06	53.9°S 279.5°E	43.8°S 174.0°E
		Data Used for the Validation of the DIC Empirical Fit			
1990	WOCE P15S	22/02/90	16/04/90	14.9°S 190°E	5.2°N 190.2°E
1992	WOCE P16aP17a	08/10/92	24/11/92	21.5°S 211.5°E	22°S 215.6°E
1993	WOCE P19c	23/02/93	10/04/93	53°S 285°E	13.5°N 268.4°E
1994	WOCE P18S	27/01/94	23/03/94	67°S 257°E	26°S 257°E
1996	WOCE P15S NOAA CGC-96	05/01/96	09/03/96	45.8°S 207°E	9.6°S 189.4°E
2001	CLIVAR P15/SR05_2001	25/05/01	04/07/01	44.4°S 180°E	2.2°S 190°E
2005	CLIVAR P16S_2005	10/01/05	11/02/05	16°S 210°E	71°S 210°E
2008	CLIVAR/CO2 P18	22/01/08	22/02/08	27.4°S 252.0°E	52.6°S 284.9°E
1974–2007	Various (LDEO)	-	-	SAZ	SAZ
		Data Used for the Validation of the pCO_2 Estimated From DIC_{fit}			
1979	Indomed Leg 15	10/02/79	05/03/79	53.4°S 289.1°E	9.0°N 280.4°E
1989	RITS/CO2–89 Leg 2	05/03/89	02/04/89	27.4°S 251.2°E	17.7°S 210.3°E
2007	Palmer 0711	14/12/07	30/12/07	52.4°S 278.6°E	46.5°S 179.3°E
2008	CLIVAR/CO2 P18	22/01/08	22/02/08	27.4°S 252.0°E	52.6°S 284.9°E
2008	Palmer 0803	09/03/08	13/03/08	77.9°S 166.6°E	46.6°S 173.5°E
2008	Palmer 0804	21/03/08	13/04/08	44.0°S 174.2°E	52.7°S 285.4°E

surface A_T measurements carried out during CLIVAR/CO2 cruise P18. The error in the A_T estimate for SST < 20°C (33 measurements) was −2.4 ± 3.6 μmol/kg. Most of the data used by *Lee et al.* [2006] in this area of the ocean were measured during summer months. We have found no winter A_T data in the region to test the accuracy of this relationship in order to use it with the wintertime CARIOCA data. An indirect approach to evaluate how well the relationship might predict wintertime A_T is to use subsurface A_T data (for depths between the mixed layer and the maximum wintertime mixed layer, 300 to 600 m, 665 data points) from the cruises listed in Table 1 and compare them with A_T estimated using equation (1). The results indicate that wintertime A_T could be lower than the estimated A_T, the difference being up to 13 μmol kg^{-1}.

2.4. Measurements of SSS and SST

[14] Measurements of salinity and temperature were carried out concurrently with pCO_2 or DIC data for the CARIOCA buoys and all the cruises.

[15] For the air-sea CO_2 flux computation, climatological SSS and SST from objectively analyzed monthly mean values [*Locarnini et al.*, 2006; *Antonov et al.*, 2006] on a 1 degree grid were obtained from the World Ocean Atlas 2005 (WOA2005) website (http://www.nodc.noaa.gov/OC5/WOA05/woa05data.html).

2.5. Estimation of Total Dissolved Inorganic Carbon

[16] No measured DIC was used but rather it was computed from A_T and pCO_2 using the solubility of CO_2 gas in seawater by *Weiss* [1974], the carbonic acid dissociation constants of *Mehrbach et al.* [1973] as refitted by *Dickson and Millero* [1987], and the boric acid dissociation constant by *Dickson* [1990]. DIC thus computed has an estimated uncertainty of ±10.5 μmol kg^{-1}, as a result of the combined uncertainties linked to the dissociation constants, the accuracy of pCO_2 measurements and the uncertainty of the alkalinity derived from the relationship proposed by *Lee et al.* [2006]. This uncertainty in the DIC estimation is mostly the result of regional biases on the A_T estimation on a scale of 1000 km. A_T estimates might also be higher than the actual A_T in the case of winter data (see section 2.3) Relative precision for successive DIC data is expected to be 0.5 μmol kg^{-1} based on the pCO_2 data from the CARIOCA [*Boutin et al.*, 2008].

[17] Validation of the empirical DIC relationship derived from these data has been carried out with ship data from cruises between 1974 and 2005 from the WOCE program and the LDEO database (Table 1 and Figure 1e).

2.6. Air-Sea CO_2 Flux Estimations

[18] The driving force of CO_2 gas exchange between the atmosphere and the ocean is usually expressed as the difference between partial pressure of CO_2 in the surface water and in the overlying air. We compute the air-sea flux (F) as follows:

$$F = k \cdot s \cdot \left(pCO_{2(sw)} - pCO_{2(atm)}\right) = k \cdot s \cdot \Delta pCO_2 \qquad (2)$$

where k represents the gas transfer velocity, s is the gas solubility coefficient (which is a well-defined function of temperature and salinity) and ΔpCO_2 is referred to as the thermodynamic driving force of the gas flux. We used weekly 1° × 1° $k \cdot s$ maps generated using Quick Scatterometer satellite (QSCAT) wind speeds as described by *Boutin et al.* [2009] and used the *Sweeney et al.* [2007] expression for wind speed dependence of gas exchange rate. The results of several recent studies converge toward a

proportionality constant about 15% lower than the original estimate of 0.31 of *Wanninkhof* [1992] [*Boutin et al.*, 2009; *Wanninkhof et al.*, 2009]:

$$k = 0.27 \cdot U^2 (660/S_C)^{0.5} \quad (3)$$

where S_C is the Schmidt number and U is 6 h mean wind speed (m s^{-1}) at 10 m above sea surface obtained from level 2B QSCAT wind speed product derived at NASA/JPL (http://podaac.jpl.nasa.gov/DATA_PRODUCT/OVW/index.html). This relationship is consistent with the $^3He/SF_6$ double tracer field measurements conducted by *Ho et al.* [2006] in the Southern Ocean. We chose the formulation by *Sweeney et al.* [2007] because they used global climate models satisfying the bomb $^{14}CO_2$ inventory which is a high-fidelity tracer for CO_2, and hence takes into account the slow rate of CO_2 gas transfer across the sea-air interface.

[19] The error in the flux estimation was computed following *Rangama et al.* [2005]. Assuming that there are only random errors and no systematic biases on the ΔpCO_2 fields, which is supported by our validation with independent data (see section 3.4), the error on the integrated flux (flux_error) can be deduced from the quadratic sum of the errors in each grid square (pixel). In this case, we use a 1 × 1° grid:

$$flux_{error} = \sqrt{\sum_{i=1}^{npixels} (K_i \cdot \Delta p_{error_i} \cdot S_i)^2} \quad (4)$$

where K_i, Δp_error_i and S_i are the CO_2 exchange coefficient, the error on ΔpCO_2 and the surface in a given pixel, respectively.

2.7. Front Detection

[20] One of the CARIOCA drifters and Palmer campaign 0804 made measurements very close to the SAF. *Boutin et al.* [2008] found that the variability of CARIOCA pCO_2 observed in the vicinity of the SAF was better described when they used a front location colocated in time with the CARIOCA measurements. Thus, the location of the SAF was estimated from altimetry data as described by *Sallée et al.* [2008]. In the case of the STF, we use the climatology from *Orsi et al.* [1995] as we are not aware of any method allowing us to detect temporal variability of the STF location applicable everywhere in the Pacific Ocean at any season. The fronts were colocated with respect to the trajectories of the drifters and the ships following the methodology described by *Boutin et al.* [2008].

2.8. Estimation of the Mixed Layer Depth

[21] ARGO float profiles were downloaded from the Coriolis Data Assembly Centre (http://www.coriolis.eu.org/cdc/argo.htm) and colocated along the trajectories of the drifters and cruises in space (±1 degree from the ship or buoy) and with a maximum time interval of 30 days between the drifter/cruise and the ARGO measurements (Figure 1d). Only measurements with quality flags 1 (good data) or 2 (probably good data) were considered.

[22] We estimated the MLD for each ARGO profile using a density criterion whereof an increase of more than 0.03 kg m^{-3} from the near surface value indicates the base of the mixed layer [*de Boyer Montégut et al.*, 2004]. MLD were grouped according to month and paired to an averaged DIC value from all CARIOCA or ship data located within the stipulated radius in the same month. A total of 220 pairs of MLD-DIC data were thus obtained (Figure 2a).

[23] *Dong et al.* [2008] compiled monthly climatologies of MLD from all available ARGO float profiles for the Southern Ocean (30°S to 60°S) using four different criteria for the estimations and based on a 1 by 1 degree grid. In order to increase colocated DIC-MLD data, we have selected the climatology based on the same density criteria of 0.03 kg m^{-3} and have associated a climatological MLD to every surface water DIC value in our data set. This raises the number of available data from the initial 220 DIC points with ARGO-derived MLD to 46000 data points with colocated climatological mixed layers (Figure 2b). The climatological MLD is similar to the MLD estimated from ARGO profiles for shallow mixed layers. For winter values and MLD deeper than 300 m, climatological MLD are on average 10% shallower than real time estimations (Figures 2a and 2b).

2.9. Chlorophyll Data

[24] CARIOCA 03740 was equipped with a fluorometer which provided a measurement of fluorescence along its trajectory but the rest of the platforms (ship or CARIOCA 01110) have no available measurements of either fluorescence or chlorophyll concentration. We used merged MODIS-SEAWIFS 8 day averaged products obtained from the NASA website (ftp://oceans.gsfc.nasa.gov/Merged/) to extract chlorophyll values (mg m^{-3}) along the trajectories of the CARIOCA drifters and Palmer cruises for comparison with our estimates. The use of daily satellite images was not appropriate because the area was often cloudy.

3. Results and Discussion

3.1. Data Description

[25] The two CARIOCA drifters deployed in the southern Pacific Ocean and the data obtained from the four Palmer cruises cover the Pacific Subantarctic Zone (SAZ) (approximately 40°S–55°S) particularly in its southern region (Figure 1c). Only data from within the SAZ, as delimited to the north by the STF and to the south by the SAF, have been considered for this study (46,000 data points). Our data set shows the surface ocean pCO_2 values to be generally undersaturated with respect to the atmospheric value, although pCO_2 data show high values close to the SAF. This frontal area is supersaturated with respect to atmospheric pCO_2 levels of 365.7 ± 4.3 μatm on average, estimated from the mole fraction of atmospheric CO_2 (xCO_2) recorded at Macquarie Island station (part of the CDIAC network for monitoring atmospheric CO_2) in 2004 and barometric pressure measured by the CARIOCA buoys.

[26] The distribution of DIC values calculated from the CARIOCA and ship pCO_2 data as described above shows regionally organized patterns (Figure 1d). High DIC values are observed in the eastern part of the SAZ close to the SAF, where deep waters are formed and deep mixed layer depths can be found [*McCartney*, 1977; *Hanawa and Talley*, 2001].

3.2. DIC-MLD Relationship and Fit

[27] The mixed layer depth in the SAZ of the Pacific Ocean can be very deep, reaching 600 m in the southeastern area close to the SAF.

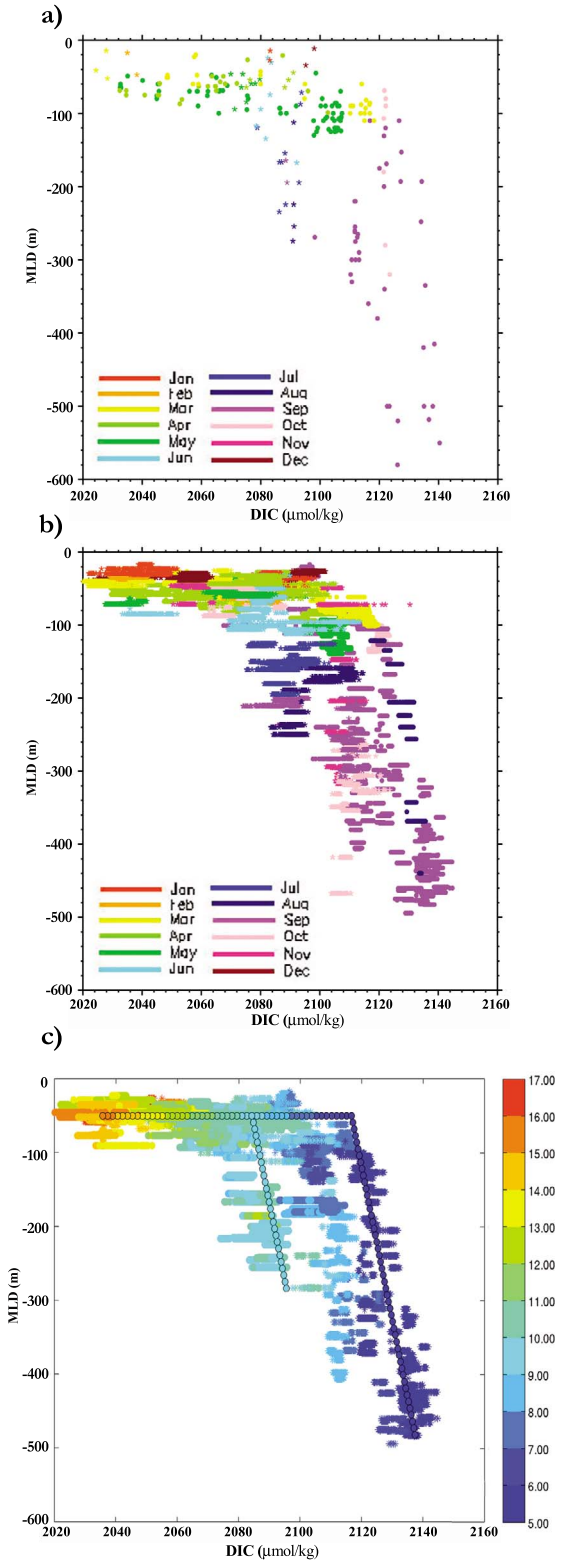

[28] The calculated DIC values were paired with MLD estimates from the ARGO profiles colocated in space and time (220 colocated data, Figure 2a) showing seasonal and longitudinal variability. Deep MLD were associated to high surface DIC values, whereas shallower MLD were associated with variable DIC values. The lowest DIC values were observed during late austral summer (March–April). The temporal data distribution was uneven; there were very few winter data (coming exclusively from the buoys) and no data at all for November. The deepest MLD were observed toward the end of the austral winter and beginning of spring, in September–October. In order to improve the number of data pairs, we associated the 46000 available DIC data points obtained from the pCO_2 data from CARIOCA and Palmer cruises with climatological MLD values for the Southern Ocean [*Dong et al.*, 2008], colocated in space and time (within ±1 degree and in the same month). This larger data set corroborates the trends observed using the ARGO colocations, with deepest MLD associated to highest DIC in late winter and variable DIC values associated to shallow MLD in austral summer (Figure 2b), that we attribute to variability in biological productivity.

[29] We observed an additional dependency of DIC with respect to SST and determined an experimental fit that allows us to calculate DIC as a function of MLD and temperature in the SAZ of the Pacific Ocean.

[30] For 4°C < SST < 18°C:

$$DIC = (2162.896 \pm 0.252) + (0.0480 \pm 0.0005) \cdot MLD - (8.097 \pm 0.020) \cdot SST \quad (5)$$

[31] The standard deviation of DIC computed from measured pCO_2 and SST-SSS-derived A_T (DIC_{calc}) with respect to DIC estimated from equation (5) (DIC_{fit}) is 9.7 μmol kg^{-1} and the correlation coefficient R^2 is 0.89. Figure 2c shows the data, color-coded for SST. For a fixed MLD (50 m) and two fixed SST (6°C and 10°C), the values calculated using our method fit well with the cloud of original data (Figure 3c). For a fixed MLD, the data represent well the range of DIC as a function of temperature. For fixed SST, the DIC follows the observed MLD-DIC_{calc} dependency. Since the empirical A_T is computed using SST there might be an issue with possible cross-correlations when comparing DIC_{calc} with DIC_{fit}, but in the Southern Ocean the influence of SST on A_T in the relationship of *Lee et al.* [2006] is weak and the weight given to SST on equation (5) is much larger than that

Figure 2. (a) MLD versus surface water DIC, color-coded for month. Stars represent CARIOCA data, diamonds indicate ship data. DIC is colocated with MLD estimated from individual ARGO float profiles. (b) Same as for Figure 2a, but using climatological MLD values. (c) MLD versus DIC color-coded for SST (°C). The horizontal plot line shows the predicted DIC values using our fit for a fixed MLD of 50 m (the circles are color-coded for temperature using the same scale). The tilted lines represent the fit for a fixed temperature of 6°C and 10°C (according to the color scale).

Table 2. Correlation Coefficients for the Parameters Used in the Estimation of DIC and pCO_2[a]

Correlations	Zero-Order		Partial	
		DIC		
SST	−0.933	DIC_{fit}	$\rho_{X1X2\cdot X3}$	−0.884
MLD	0.718		$\rho_{X1X3\cdot X2}$	0.430
Salinity	−0.322	-	$\rho_{X1X4\cdot X2X3}$	0.545
		pCO_2		
SST	−0.499	$pCO_{2\text{-MLD}}$	$\rho_{X5X2\cdot X3}$	−0.276
MLD	0.489		$\rho_{X5X3\cdot X2}$	0.254
SST	−0.499		$\rho_{X5X2\cdot X3X4}$	−0.175
MLD	0.489	$pCO_{2\text{-SSS}}$	$\rho_{X5X3\cdot X2X4}$	0.261
Salinity	−0.246		$\rho_{X5X4\cdot X2X3}$	−0.072
DIC	0.716	-	$\rho_{X5X1\cdot X2X3X4}$	0.994

[a]The results are all statistically significant with p = 0.000. In $\rho_{XiXj\cdot Xz}$: X_1 is DIC, X_2 is SST, X_3 is MLD, X_4 is salinity and X_5 is pCO_2. $pCO_{2\text{-MLD}}$ is pCO_2 estimated from MLD and SST, and $pCO_{2\text{-SSS}}$ is estimated from MLD, SST and SSS.

for A_T. For example, an increase of 1°C from the mean SST in the data set (9.9°C), would lead to an increase in A_T of 2 μmol kg^{-1} whereas DIC_{fit} would decrease by 8 μmol kg^{-1}. The influence of SST is 4 times larger in magnitude and in opposite sense in DIC_{fit} than in A_T.

[32] We have estimated the multiple partial correlations of DIC with respect to SST and MLD (Table 2). The coefficient for SST indicates that it has a strong linear relationship with DIC which is not substantially altered once the influence of MLD is removed (the zero-order and partial coefficients are similar). In the case of MLD and DIC we also find a significant linear relationship between both, but the partial correlation coefficient, though still significant is about 40% smaller than the zero-order coefficient (0.430 compared to 0.718), indicating that SST plays a role in the relationship between DIC and MLD.

[33] We also tested including weekly averaged MODIS-SEAWIFS chlorophyll concentration as an additional proxy in our algorithm, using the 29900 colocated DIC-Chl available but this did not improve R^2 (0,88) or σ^2 (10,4) so we retain equation (5).

3.3. Small-Scale Variability: Biological Activity

[34] Highly variable DIC_{calc} values are observed with respect to the fit during austral summer (Figure 2). We examine to which extent biological production is responsible for the observed variability. Diel cycles of high-frequency CARIOCA measurements of DIC_{calc} and pCO_2 in the southern Atlantic and Indian Oceans as well as the North Atlantic have already been observed and used to derive biological production rates [*Boutin and Merlivat*, 2009; *Merlivat et al.*, 2009]. We followed the method described by these authors for estimating net community production (NCP) from DIC estimates in the Pacific SAZ. This method estimates biological production from pCO_2 measurements made in situ from unattended platforms using a nonintrusive method.

[35] Several short periods with diurnal cycles of DIC_{calc} phased with sun light and SST and without significant variation of SSS were detected between November 2004 and February 2005 for buoys 03740 and 01110 (Table 3). During the austral spring and summer, the MLD becomes shallower as the season progresses. A warm, isolated layer may form during the daylight period. When no significant change in SSS is observed, vertical mixing and thus the DIC flux through the base of the mixed layer, and advection may be neglected. Additionally, when the daily maximum in DIC is phased with sunrise and the minimum is observed in phase with the sunset, we identify biological activity as the main factor responsible for the observed DIC variability. During the second part of the day, nocturnal convection mixes the warm layer within the mixed layer [*Brainerd and Gregg*, 1995], so that the DIC value at sunrise is considered as representative of a homogeneous mixed layer value.

[36] According to *Boutin and Merlivat* [2009], the Net Community Production, NCP on a diurnal scale can be calculated from:

$$NCP = \frac{\Delta C}{\Delta t} + \frac{1}{\rho}\cdot\frac{F}{h} \tag{6}$$

where F is the air-sea CO_2 flux, h is the depth of the mixed layer, ρ is the density of seawater and $\Delta C/\Delta t$ is the change of DIC between two consecutive maxima (between two sunrises). Mixed layer depths were computed from ARGO profiles colocated with the position of the drifters. We also identify in detail the daily variation in DIC ($(C_M\text{-}C_m)$, Table 3) and then calculate NCP [e.g., *Boutin and Merlivat*, 2009, Figure 3e].

[37] Table 3 summarizes the results obtained for all the periods selected. The daylight decrease in DIC ($C_M\text{-}C_m$) ranges from 2.2 to 6.6 μmol kg^{-1}. Given that the relative precision between consecutive calculated DIC data points is 0.5 μmol/kg [*Boutin et al.*, 2008], these variations are significant and not the result of the error in the estimation. In the case of the 6.6 μmol kg^{-1}, the signal in DIC is clear, SSS

Table 3. Biological Activity Derived From Periods Between November 2004 and January 2005 When Diurnal Cycles Were Observed[a]

Time	Buoy	Days	Location	$C_M\text{-}C_m$ (μmol kg^{-1})	$\Delta C/\Delta t$ (μmol kg^{-1}d^{-1})	$F_{air\text{-}sea}$ (mmol m^{-2}d^{-1})	h (m)	NCP (μmol kg^{-1}d^{-1})	Chl-a (mg m^{-3})
5–8/11	03740	3	51°S to 140°W	5.32 ± 0.76	1.69 ± 0.20	2.38	200	1.70 ± 0.20	0.22
30/11–1/12	03740	2	49°S to 135°W	2.79 ± 0.78	0.52 ± 0.54	2.17	50	0.56 ± 0.54	0.27
16–20/12	03740	3	49°S to 131°W	3.83 ± 0.50	1.29 ± 0.61	4.34	60	1.36 ± 0.61	0.31
25–28/12	01110	3	46°S to 151°W	6.61 ± 1.14	4.75 ± 0.28	7.70	50	4.90 ± 0.28	0.38
18–21/1	03740	3	48.5°S to 126°W	2.21 ± 0.59	0.63 ± 0.65	6.48	45	0.77 ± 0.65	0.14
29–30/1	03740	2	48.5°S to 124°W	4.03 ± 0.92	1.34 ± 0.33	7.71	45	1.51 ± 0.33	0.14

[a]Abbreviations are as follows: h, the MLD estimated from ARGO profiles; $(C_M\text{-}C_m)$, the difference between the maximum and the minimum of DIC during daylight (as defined by *Boutin and Merlivat* [2009]).

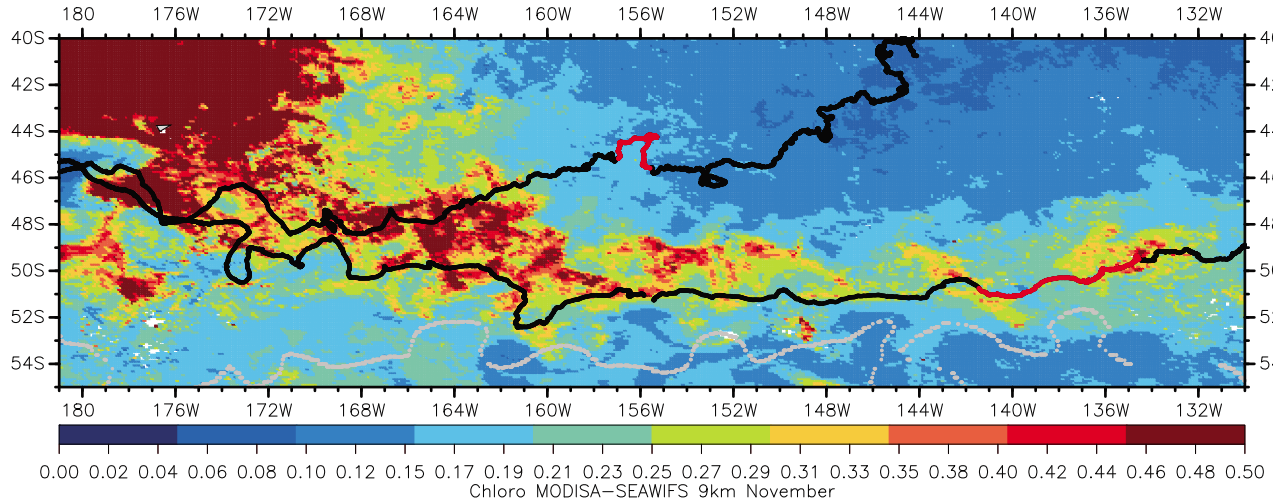

Figure 3. CARIOCA trajectories (01110 is the buoy further north, 03740 is the one in the south) superimposed on a combined MODIS-SEAWIFS monthly averaged chlorophyll image in November 2004. The chlorophyll concentration is expressed in mg m^{-3}. The red section of the trajectories indicates the location of the buoy in the month represented.

does not change and the warming superposed to the diurnal variability observed in the SST confirms that the conditions needed to estimate NCP using equation (6) apply. This is true in particular on 27 December, where the variation in SST is close to 1°C. NCP values in December–January vary between 0.56 and 4.90 μmol kg^{-1} d^{-1}. This large value must be interpreted as an episodic event measured at the time scale of 3 days.

[38] Chlorophyll-a concentrations in the Subantarctic Zone of the Pacific Ocean remain low ($\leq$0.3 mg m^{-3}) between November and February except in coastal areas and north of the SAF (Figure 3 and Table 3). In November, buoy 03740 was able to detect several diurnal cycles of DIC. The buoy was at the time drifting along a tongue of increased chlorophyll, probably related to the vicinity of the SAF. We colocated the satellite chlorophyll values with the trajectory followed by the buoys and found the average chl-a concentration for the periods where diurnal cycles were observed (Table 3). We found no significant relationship between satellite chlorophyll concentration and biological activity detected through the diurnal cycles of DIC_{calc}. These results are in good agreement with *Rangama et al.* [2005], who also found that for data in the Southern Ocean south of Tasmania and New Zealand a chlorophyll threshold of 0.37 mg m^{-3} marks the limit for which satellite-derived chlorophyll correlates well with pCO_2. Thus, biological activity alone cannot explain the variations in DIC levels between the northern and the southern part of the SAZ.

3.4. Validation of the DIC Fit With Independent Data and pCO_2 Estimation

[39] The robustness of the fit has been tested against a set of independent DIC surface measurements obtained from WOCE and CLIVAR sections P15 to P19 as well as additional cruises carried out by the group at LDEO spanning from 1974 to 2008 (Table 1 and Figures 1e and 4). A total of 537 DIC measurements from this independent data set, with associated SST between 4°C and 18°C, have been compared against their corresponding DIC_{fit} estimates, with an error in the estimate of -8.3 ± 11.8 μmol kg^{-1} with respect to the in situ measurements. When the DIC observations are normalized to the year 2005 assuming an annual increase of 1 μmol kg^{-1} due to invasion of anthropogenic CO_2, a better correspondence of 1.0 ± 9.9 μmol kg^{-1} is obtained. Given the number of measurements, and a σ of 9.9 μmol kg^{-1}, the relative precision on the mean difference, estimated as the standard deviation of the mean $(9.9/(N-1)^{0.5}$, where N =

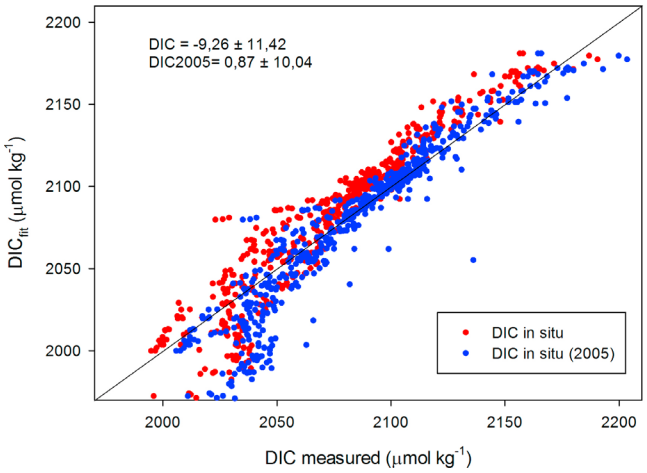

Figure 4. DIC measurements from WOCE and CLIVAR cruises from 1974 to 2008, with associated SST between 4°C and 18°C compared to DIC estimates using the fit. In red, actual DIC measurements; in blue, DIC measurements normalized to 2005 assuming an annual increase of 1 μmol kg^{-1}.

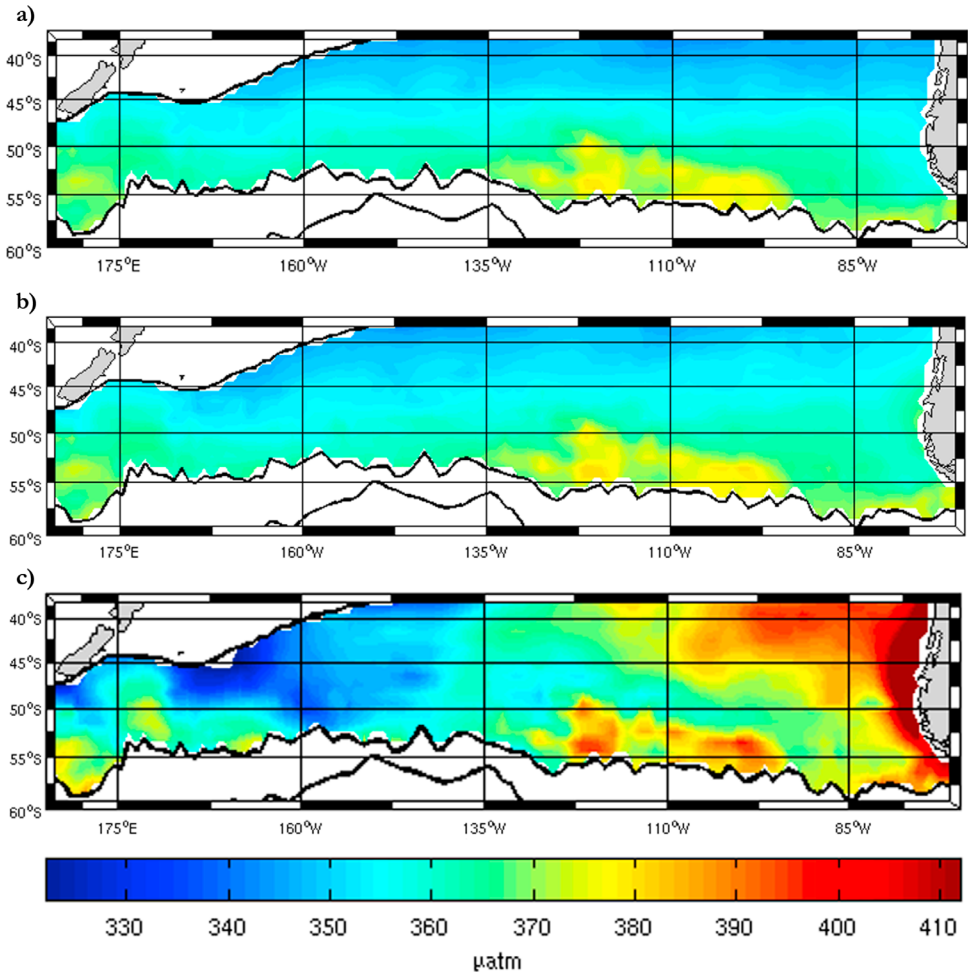

Figure 5. The pCO_2 (μatm) calculated for July using the (a) $pCO_{2\text{-MLD}}$ fit, based on MLD and SST; (b) $pCO_{2\text{-SSS}}$ fit, based on MLD, SST and salinity; and (c) $pCO_{2\text{-DIC}}$ fit, estimating pCO_2 from DIC-A_T pairs, where DIC is calculated from MLD and SST and A_T is calculated following *Lee et al.* [2006].

537), is 0.4 μmol kg^{-1}. The change in the bias is consistent with the change in DIC due to the time elapsed between the cruises and 2005, which would be on the order of a decade.

[40] We next compute pCO_2 from this DIC_{fit} and the empirical A_T, ($pCO_{2\text{-DIC}}$). The error in the estimation is ±17.8 μatm. We also applied a multiple linear regression (MLR) approach to test the use of a fit to estimate pCO_2 directly from MLD and SST ($pCO_{2\text{-MLD}}$) and from MLD, SST and SSS ($pCO_{2\text{-SSS}}$). Although the standard deviations were slightly better for $pCO_{2\text{-MLD}}$ and $pCO_{2\text{-SSS}}$, 16.2 and 16.4 μatm, respectively, these fits did not show regional variability as observed in the SAZ of the Pacific Ocean with $pCO_{2\text{-DIC}}$ (Figure 5). Additionally, we estimated the partial correlation coefficients for the different pCO_2 fits we tested (Table 2). All the parameters considered contribute significantly to the prediction of pCO_2. SST and MLD have a similar contribution in the prediction of pCO_2, whereas salinity plays a smaller role. The partial correlation coefficients for $pCO_{2\text{-MLD}}$ and $pCO_{2\text{-SSS}}$ are all substantially lower than the zero-order coefficients, indicating that the different parameters enhance each other's role in the determination of pCO_2. DIC is the only parameter whose relationship with pCO_2 increases when the effects of the others are removed and overall is the variable that contributes the most to the estimation of pCO_2. As we will show later when validating pCO_2 with in situ data in the eastern region, the algorithms applied to determine the DIC_{fit}, and then estimate the $pCO_{2\text{-DIC}}$ reflect the physical mechanisms in the region much better than the linear fits used to compute either $pCO_{2\text{-MLD}}$ or $pCO_{2\text{-SSS}}$, and they can represent the areas of water mass formation more accurately. This can be explained due to the fact that the MLR used for $pCO_{2\text{-MLD}}$ and for $pCO_{2\text{-SSS}}$ cannot reproduce the complex, nonlinear dynamics of the carbon system. If we look at $pCO_{2\text{-SSS}}$ and $pCO_{2\text{-DIC}}$ (Figures 5b and 5c, respectively), in both cases the number of independent variables used is ultimately the same (MLD, SST, and SSS). The difference lies in the way that salinity is considered. In the first case, it is introduced directly in the MLR and the resulting fit gives SSS a coefficient of −0.8 μatm pss^{-1}. In the case of $pCO_{2\text{-DIC}}$, SSS is introduced in the estimation of A_T in a quadratic expression and pCO_2 is then estimated using the equilibrium carbon chemistry

relationships, which are also highly nonlinear. This results in a much higher influence of SSS on $pCO_{2\text{-DIC}}$, such that for a given DIC_{fit}, the change in $pCO_{2\text{-DIC}}$ as a result of changes in SSS is an order of magnitude higher. This nonlinearity is what improves the representation of the physical structures observed in Figure 5c. Consequently, we chose the $pCO_{2\text{-DIC}}$ fit.

[41] We validated our method against independent pCO_2 measurements obtained in campaigns spanning from 1979 to 2008 doing basin-wide cruises (Palmer-0711 and Palmer-0804 [*Takahashi et al.*, 2009b]) and north-south transects (in the west, south of New Zealand, Palmer-0803, and in the eastern part of the SAZ, Indomed leg 15, RITS/89-CO2 and the repeat hydrography CLIVAR/CO2 P18 cruise, from the CDIAC database) in different seasons and years (Table 1 and Figure 1e). We have corrected these data to 2005 assuming a pCO_2 increase rate which follows that of the atmospheric pCO_2 (1.7 μatm yr^{-1}). Our $pCO_{2\text{-DIC}}$ compares well with the values recorded in cruises; the average difference between the measurements and our estimates is 2.4 ± 13.5 μatm. We split the validation data into two independent sets (before and after 2005 with 283 and 20,884 data points, respectively) to determine whether there is a trend with respect to our estimates (Figure 6a). No significant trend could be deduced because regional differences mask possible trends. For a better analysis we focus only on the eastern north-south transects, cruises Indomed leg 15 and RITS/89-CO2 from before 2005 (283 data points) and CLIVAR/CO2 P18 from after 2008 (3480 data points). The average differences found with respect to the estimates are −2.3 ± 6.3 μatm and −1.0 ± 16.1 μatm, respectively. These three cruises carried out in the eastern part of the SAZ are those where the biggest differences are observed in the pCO_2 estimates and in the air-sea CO_2 fluxes (sections 3.5 and 3.6). Figure 6 shows the pCO_2 measured during these cruises without coastal data, normalized to the year 2005. We compare the normalized measurements to the values estimated using our method and to the pCO_2 from the climatology by *Takahashi et al.* [2009a], referred to as Taka09, for the months when the cruises took place, and extracted along their tracks. All the cruises observed a similar increase in pCO_2 in the area between 50°S and 42°S. Our method was able to predict pCO_2 values which were close to the actual measurements in the cases of Indomed-15 and RITS/89 up to 42°S (Figures 6b and 6c). Although the fit predicts higher pCO_2 than Taka09 in the region from 50°S northward, the estimates are still lower than the actual measurements. In the case of CLIVAR/CO2-P18 cruise (Figure 6d), both our estimates and those from Taka09 fail to correctly reproduce the experimental record. SST values recorded during this cruise indicate that it was an unusually warm year, with a mean difference with respect to the WOA2005 temperatures of 2.5°C, which can help explain the differences observed. We have used our $pCO_{2\text{-DIC}}$ fit to calculate pCO_2 using actual SST and salinity values and MLD (computed from stations sampled during P18). The pCO_2 thus obtained for January 2008 (Figure 6d, purple line) is closer to the observed underway pCO_2 measurements, particularly south of 45°S.

3.5. Monthly CO_2 Flux Maps

[42] Objectively analyzed monthly mean values of temperature and salinity from WOA2005 were used in combination with the monthly values of MLD from the climatology by *Dong et al.* [2008] to create monthly maps of DIC (using equation (5)), pCO_2 and air-sea CO_2 fluxes (using equation (2)) (Figures 7d, 7e, and 8d). For comparison purposes, only January and July are shown. The complete climatology for the SAZ of the Pacific Ocean can be found in the auxiliary materials section.[1] The DIC maps show high values close to the SAF and along the Chilean coast, particularly during austral winter (July) when the vertical mixing is enhanced and the Subantarctic Mode Water and Antarctic Intermediate Water are formed [*McCartney*, 1977; *Talley*, 1999; *Sallée et al.*, 2008].

[43] Overall, the Pacific SAZ acts as a weak sink for atmospheric CO_2, absorbing an estimated 0.05 ± 0.03 PgC yr^{-1} (Table 4). The flux maps show that the southeastern part of the SAZ, close to the SAF acts as a source of CO_2 especially during winter. Our method also shows high pCO_2 values close to the South American continent, in the area between 55 and 40°S (Figure 7e) all yearlong and consequently, this region acts as a source of CO_2 throughout the year. These high pCO_2 values are related to the shallow salinity minimum observed in the area and which has been associated to a possible influence of the formation of Antarctic Intermediate Water [*Leth et al.*, 2004]. In areas closer to the Chilean coast (up to approximately 100 km offshore) from 40°S northward, an upwelling takes place during the summer which could also contribute to the high pCO_2 observed in the northernmost part of the area [*Letelier et al.*, 2009].

3.6. Comparison With Other Flux Estimates

[44] We have compared our results with other available flux climatologies in the area (Figures 8 and 9). Using the ΔpCO_2 maps from three previous estimations [*McNeil et al.*, 2007, McN07; *Boutin et al.*, 2008, Boutin08; Taka09], we have calculated the air-sea CO_2 fluxes in the SAZ of the Pacific Ocean in 2005 for each case, with the same winds and CO_2 exchange coefficient used in our estimations (see section 2.6). Table 4 summarizes the data sets and approaches used by the authors for each ΔpCO_2 climatology as well as our new flux estimation obtained for the SAZ of the Pacific Ocean in each case. Our results differ the most from McN07, although they find a source region close to the front, as our results suggest, and from Boutin08. McN07 suggest that the Pacific Ocean was the region for which their method needed further analyses in order to determine whether the signal observed was realistic. Boutin08 propose a method for estimating fluxes based on the distance to the SAF, mostly based on measurements taken in the vicinity of the SAF in regions other than the eastern Pacific Ocean. This method is not able to correctly detect variability linked to deep water formation. Our results are closer to those proposed by Taka09, who find a region close to equilibrium near the SAF

[1] Auxiliary materials are available at ftp://ftp.agu.org/apend/gb/2010GB003818.

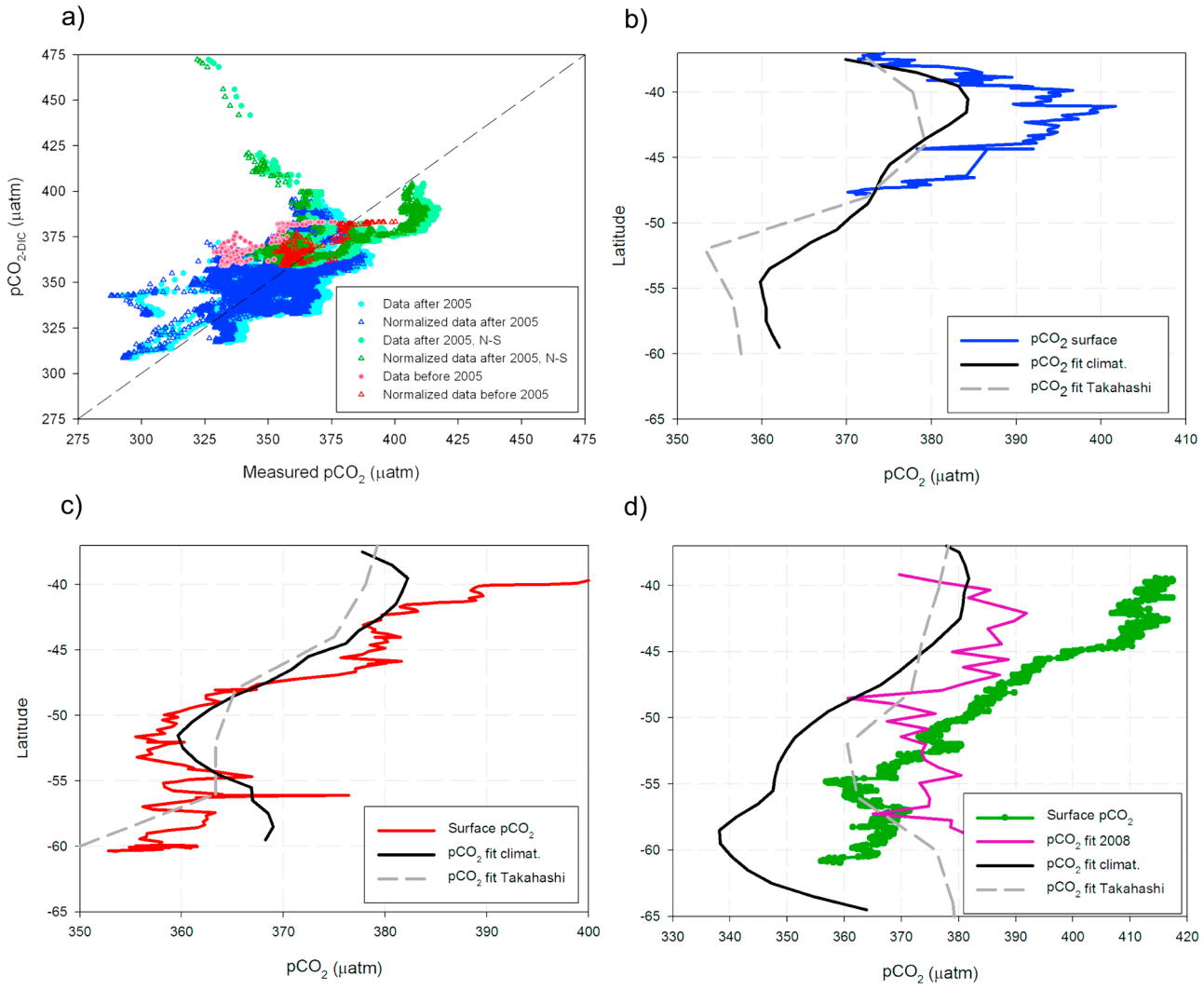

Figure 6. (a) The pCO_2 from validation cruises carried out before 2005 (filled red circles), after 2005 (filled blue circles) and after 2005 but only in the north-south transect (filled green circles) compared to our pCO_2 estimates. Also represented with the same color code are the same data normalized to the year 2005 (red, blue, and green triangles) assuming an annual increase of 1.7 μatm. (b) The pCO_2 (μatm) measured during Indomed leg 15 in February 1979 normalized to 2005 assuming a constant increase of 1.7 μatm yr^{-1} following the atmospheric trend (blue), calculated along 97°W with our fit (black) and extracted from Taka09's climatology (dashed gray line) for February. (c) Same as before for cruise RITS/89-CO2 in March 1989 (red). The pCO_2 estimates correspond to March, along 105°W. (d) Same as before for cruise CLIVAR/CO2 cruise P18 in January 2008 (green). The estimates correspond to January, along 103°W. The purple plot shows the pCO_2 calculated through our fit using the SST, MLD and salinity from stations sampled during CLIVAR/CO2 P18 instead of the climatological values.

and a weak sink in the western part of the SAZ, although they predict a higher overall sink because their method does not reproduce the high pCO_2 areas associated with deep water mass formation regions in the eastern part of the Pacific SAZ. Thus, the source area west of the South American continent is ultimately responsible for the difference we find in our estimations with respect to previous climatologies of the area, which estimated considerably larger CO_2 sinks in the Pacific SAZ (McN07: −0.5 PgC yr^{-1}, Boutin08: −0.5 PgC yr^{-1} and Taka09: −0.16 PgC yr^{-1}, Table 4). We calculated the integrated air-sea CO_2 flux in the SAZ of the Pacific Ocean on a monthly basis (Figure 9) for each climatology. McN07 and Boutin08 show the area as a strong sink of CO_2 throughout the year. Taka09 show the area as a weak sink all through the year while our method suggests a seasonal cycle in which the SAZ is close to equilibrium with the atmosphere or is a weak source during winter, and acts as a sink toward the end of winter, and in

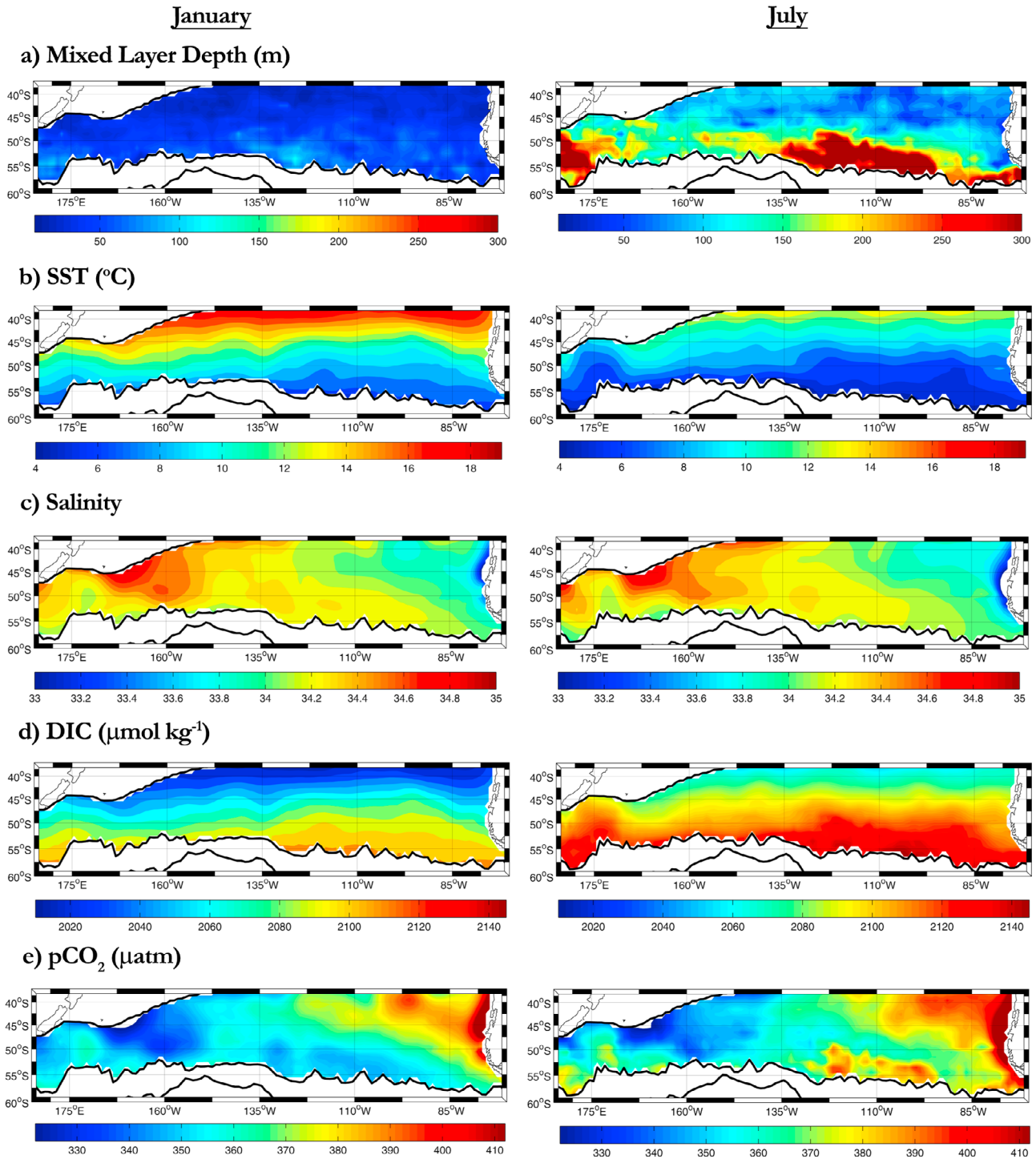

Figure 7. (a) Mixed layer depth in m (from the climatology by *Dong et al.* [2008]), (b) sea surface temperature in °C (from WOA2005), (c) salinity (from WOA2005), (d) DIC (μmol kg^{-1}), and (e) pCO_2 (μatm) for the months of (left) January and (right) July in the SAZ of the Pacific Ocean. DIC and pCO_2 have been estimated using our fit.

spring and summer as a result of biological activity in the area. Our method therefore is able to predict a realistic seasonal variation throughout the year. The biggest differences between our approach and that of Taka09 are observed in austral winter (Figures 8 and 9), where Taka09 present a relatively homogeneous situation in all the SAZ while the $pCO_{2\text{-DIC}}$ fit shows a stronger CO_2 source in the eastern Pacific.

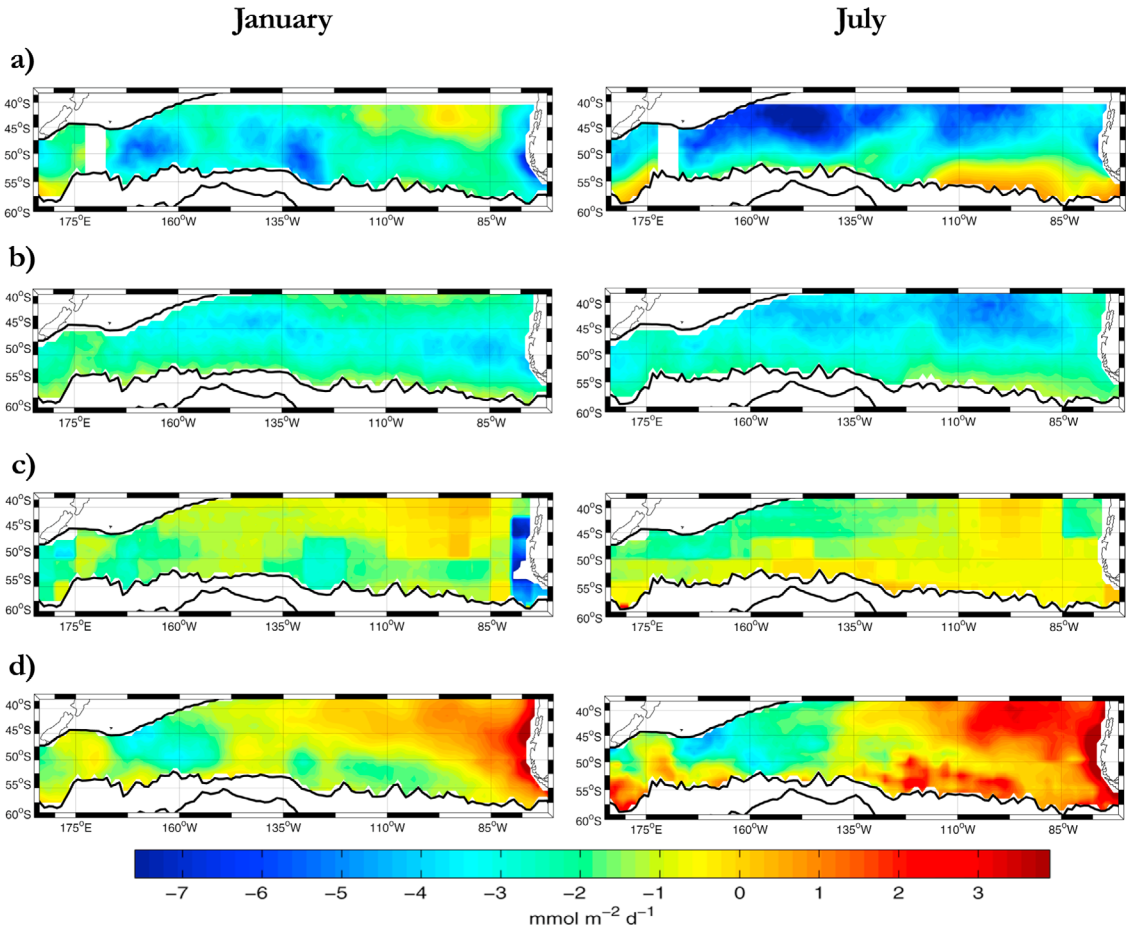

Figure 8. Air-sea CO_2 flux in the SAZ of the Pacific Ocean in (left) January and (right) July 2005 according to (a) McN07, (b) Boutin08, (c) Taka09, and (d) this study.

3.7. Evaluating Interannual Variability

[45] The sampling in the southern Pacific Ocean has been sparse and irregular so far and interannual variability and decadal changes in the CO_2 uptake rate are difficult to determine based only on the existing measurements. This is why variability in the area has been studied mainly through models so far. We have studied interannual variability in the pCO_2 and DIC measurements available by estimating the residuals for all the data (Figure 10a). The trends we obtain are 2.04 μatm yr^{-1} and 5.18 μmol kg^{-1} yr^{-1}. While the trend for pCO_2 is consistent with the climatological mean rates estimated by Taka09, the trend in DIC is unrealistically high compared to other estimates [*Takahashi et al.*, 2009a; *Le Quéré et al.*, 2010]. In any case, they are both very small compared to the variability observed for any given year, which can be as large as 100 μatm or μmol kg^{-1}, respectively. This variability is the result of regional differences within the Pacific SAZ. Therefore, we think that at this point it is not possible to determine pCO_2 uptake rates in the area using the available data.

Table 4. Approaches for the CO_2 Flux Estimation in the Southern Ocean[a]

Study	Method	Region	Data	Pacific SAZ Estimate
McNeil et al. [2007]	DIC as a function of SST, SSS, O_2, NO_3 and SiO_4; A_T as a function of SSS, NO_3 and SiO_4	Southern Ocean	DIC ship data (1986–1997)	0.51 PgC yr^{-1}
Boutin et al. [2008]	pCO_2 as a function of distance to SAF	Global SAZ	Carioca in eastern Atlantic, Indian and western Pacific (2003–2006)	0.50 PgC yr^{-1}
Takahashi et al. [2009a]	Measured seawater pCO_2 extrapolated using an advection-diffusion transport model	Global Ocean	Ship data (1970–2007)	0.16 PgC yr^{-1}
This work	DIC as a function of MLD and SST; A_T as a function of SST and SSS	Pacific Ocean SAZ	Ship and Carioca in Pacific SAZ (1979–2008)	0.05 PgC yr^{-1}

[a]The estimates for McN07, Boutin08 and Taka09 have been recalculated using the ΔpCO2 fields provided by the authors and then using the same winds and gas exchange coefficient as for our study. The values reflect the flux only in the SAZ of the Pacific Ocean, as defined in this work.

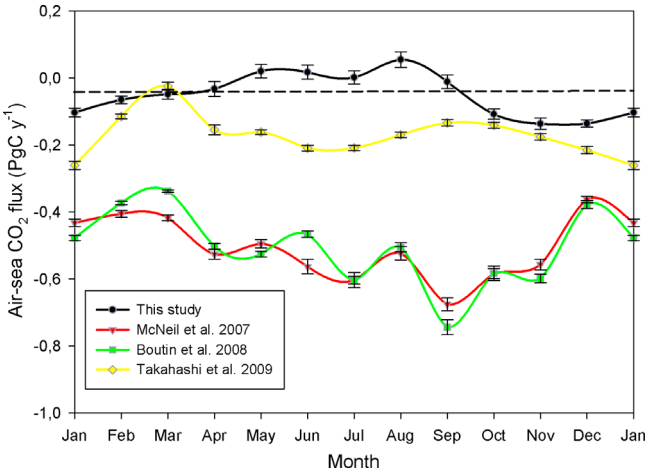

Figure 9. Monthly averaged integrated air-sea CO_2 flux (PgC yr^{-1}) on the SAZ of the Pacific Ocean according to the different methods compared: McN07 (red), Boutin08 (green), Taka09 (yellow), and this work (black). The error bars show the standard deviation of the estimated monthly means.

[46] In the Southern Ocean, the dominant mode of atmospheric interannual variability is the Southern Annular Mode (SAM). A positive SAM strengthens the westerlies and is also associated with a poleward shift of these winds. Given the influence of wind stress in the air-sea gas exchange, a positive SAM will affect the CO_2 system in the SAZ, enhancing outgassing [*Lovenduski et al.*, 2007]. Although measurements show that the spatial variability of DIC between the eastern and western sectors in the Pacific SAZ is more than 50 μmol kg^{-1} (Figures 1 and 10a) while the SAM influence is on the order of a few μmol kg^{-1} [*Lovenduski et al.*, 2007], we tested which DIC anomaly our DIC_{fit} (equation (5)) would predict during a SAM event. *Sallée et al.* [2010] have recently published a study about the response of the MLD to the SAM using data from ARGO profiles. We use their MLD and SST anomaly fields regressed onto the SAM (their Figure 4) with our DIC_{fit} to estimate the expected DIC anomaly induced by the SAM (Figure 10b). Our results show positive anomalies between 135°W and 105°W and negative anomalies elsewhere. The DIC anomalies in the Pacific SAZ are anticorrelated with SST and correlated with MLD anomalies. This is in agreement with the model results from *Lovenduski et al.* [2007]. The MLD anomalies affect DIC anomalies mostly close to the SAF, everywhere else the DIC anomalies are determined by SST.

[47] In any case, the influence of the SAM on DIC is again small compared to the total variability observed in our data set. More data from repeat sections over the years will be needed to fully determine the effect of the SAM on DIC in the Pacific SAZ.

4. Conclusions

[48] Surface data from the CARIOCA drifters and the ships in the SAZ of the Pacific Ocean show an organized pattern in calculated DIC, which decreases from the SAF to the STF. This suggests mixing of surface and deep waters close to the SAF resulting in richer DIC content. High DIC values are shown to be related to deep MLD (in early spring). Deepest MLD and highest DIC are observed in September–October in the eastern Pacific, close to the SAF. During the summer, shallower MLD are associated with a wider range of DIC values, with lowest values observed in late summer (March). Regionally, higher DIC and deeper MLD are observed east of 140°W during austral summer.

[49] We associate the variability observed in DIC during the summer to the role of biological activity in the area. We were able to detect diurnal cycles in the DIC data set of the CARIOCA drifters on average 1 out of every 3 days during summer. Fewer diurnal cycles were detected for buoys 01110 and 03740 in the southern Pacific Ocean than were found in the study carried out by *Boutin and Merlivat* [2009] in the southern Atlantic Ocean, perhaps because this study was carried out in the Polar zone, yet the results obtained show similar biological activity whenever the diurnal cycles are observed. Through the use of the hourly measurements provided by the CARIOCA drifters, we estimate net community production. We find no direct correlation between our NCP estimates and 8 day averaged SEAWIFS-MODIS combined satellite chlorophyll images for low chlorophyll concentrations.

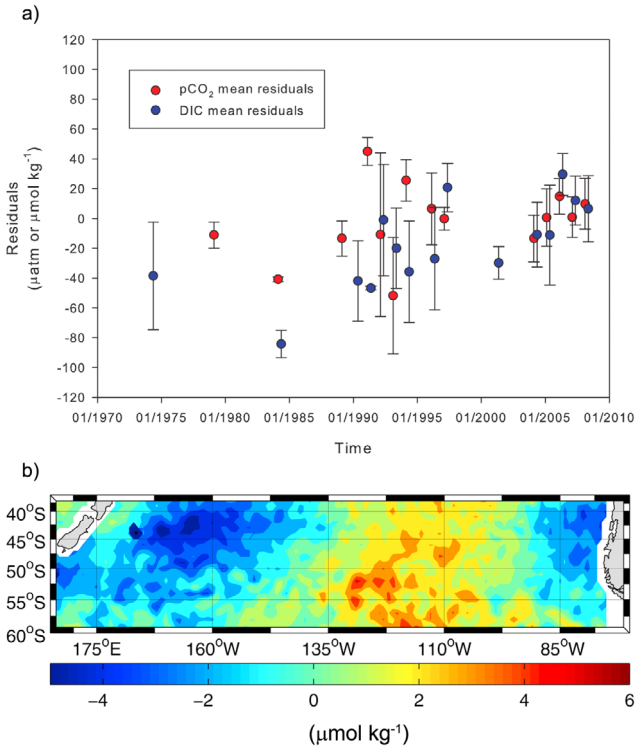

Figure 10. (a) Annual mean and standard error residuals of pCO_2 (in red, μatm) and DIC (in blue, μmol kg^{-1}) with respect to time computed for our database and the validation cruises. (b) Estimated DIC regressed onto the SAM (μmol kg^{-1}) in the southern Pacific Ocean between 30°S and 60°S.

[50] We propose a method that estimates the air-sea CO_2 flux in the SAZ of the Pacific Ocean based on estimating DIC using MLD and SST which we have validated against independent measurements dating from 1979 to 2008. Previous studies have failed to correctly represent the regions of deep water mass formation in the SAZ. We combined previously used ship data with CARIOCA measurements in the area, which provide data from otherwise unsampled months to complete an annual record of measurements. Having monthly data, particularly in winter, allowed us to detect a relationship between DIC, MLD and SST through which we were able to derive CO_2 fluxes taking into consideration the source areas associated to formation regions. The use of an MLR technique to directly estimate pCO_2 from SST and MLD or SST, SSS and MLD alone was also not able to capture the higher pCO_2 in these formation regions. Our $pCO_{2\text{-DIC}}$ fit, on the other hand, correctly predicts the physical mechanisms observed in the area. It also predicts the existence of a seasonal cycle in the air-sea CO_2 fluxes in the SAZ of the Pacific Ocean. The area is a sink during spring and summer and is close to equilibrium or a weak source in winter. The Pacific SAZ acts as a sink for atmospheric pCO_2 on an annual scale (0.05 ± 0.03 PgC yr^{-1}) and our estimations indicate that it is a weaker sink than previously suggested by other authors. Although data from different decades are available, large regional and seasonal variability complicates the study of interannual variability. More repeat hydrographies and biogeochemical observations in various seasons are needed in order to determine changes in CO_2 uptake rates and the exact influence of the SAM in this area.

[51] **Acknowledgments.** This work has been funded through the European Integrated Project CARBOOCEAN (contract 511176). The pCO_2 system aboard the RVIB Palmer was designed and maintained by T. Newberger and C. Sweeney, and the DIC measurements for Palmer samples were made by J. Goddard. The work aboard the Palmer was supported by grants to T. T. from U. S. National Oceanographic and Atmospheric Administration (NOAA) and National Science Foundation (NSF). The P18 cruise was part of the CLIVAR/CO2 program cosponsored by NOAA and NSF with J. Bullister and G. Johnson as chief scientists and R. Feely and R. Wanninkhof as PIs in charge of DIC and pCO_2 measurement. The Pacific WOCE cruises were funded by NSF, NOAA, and the U.S. Department of Energy. We acknowledge the generous data contributions of numerous authors to the CDIAC database which we used for our method validation as well as for atmospheric xCO_2 from Macquarie Island. The authors would also like to thank the Coriolis data assembly center for providing the ARGO profiles used in this work. QuikSCAT K fields were obtained from the CERSAT/IFREMER ftp site (ftp.ifremer.fr). Finally, the authors thank J.B. Sallée for providing the MLD and SST anomaly fields regressed onto the SAM. This work has benefited from the contribution of two anonymous reviewers.

References

Antonov, J. I., R. A. Locarnini, T. P. Boyer, A. V. Mishonov, and H. E. Garcia (2006), *World Ocean Atlas 2005*, vol. 2, *Salinity*, *NOAA Atlas NESDIS 62*, edited by S Levitus, 182 pp., U.S. Govt. Print. Off., Washington, D. C.

Bates, N. R., L. Merlivat, L. Beaumont, and A. C. Pequignet (2000), Intercomparison of shipboard and moored CARIOCA buoy seawater fCO(2) measurements in the Sargasso Sea, *Mar. Chem.*, *72*(2–4), 239–255, doi:10.1016/S0304-4203(00)00084-0.

Boutin, J., and L. Merlivat (2009), New in situ estimates of carbon biological production rates in the Southern Ocean from CARIOCA drifter measurements, *Geophys. Res. Lett.*, *36*, L13608, doi:10.1029/2009GL038307.

Boutin, J., L. Merlivat, C. Henocq, N. Martin, and J. B. Sallée (2008), Air-sea CO_2 flux variability in frontal regions of the Southern Ocean from Carbon Interface Ocean Atmosphere drifters, *Limnol. Oceanogr.*, *53*(5), 2062–2079, doi:10.4319/lo.2008.53.5_part_2.2062.

Boutin, J., Y. Quilfen, L. Merlivat, and J. F. Piolle (2009), Global average of air-sea CO_2 transfer velocity from QuikSCAT scatterometer wind speeds, *J. Geophys. Res.*, *114*, C04007, doi:10.1029/2007JC004168.

Brainerd, K. E., and M. C. Gregg (1995), Surface mixed and mixing layer depths, *Deep Sea Res., Part I*, *42*(9), 1521–1543, doi:10.1016/0967-0637(95)00068-H.

Canadell, J. G., C. Le Quéré, M. R. Raupach, C. B. Field, E. T. Buitenhuis, P. Ciais, T. J. Conway, N. P. Gillett, R. A. Houghton, and G. Marland (2007), Contributions to accelerating atmospheric CO_2 growth from economic activity, carbon intensity, and efficiency of natural sinks, *Proc. Natl. Acad. Sci. U. S. A.*, *104*(47), 18,866–18,870, doi:10.1073/pnas.0702737104.

Copin-Montegut, C., M. Begovic, and L. Merlivat (2004), Variability of the partial pressure of CO_2 on diel to annual time scales in the northwestern Mediterranean Sea, *Mar. Chem.*, *85*(3–4), 169–189, doi:10.1016/j.marchem.2003.10.005.

de Boyer Montégut, C., G. Madec, A. S. Fischer, A. Lazar, and D. Iudicone (2004), Mixed layer depth over the global ocean: An examination of profile data and a profile-based climatology, *J. Geophys. Res.*, *109*, C12003, doi:10.1029/2004JC002378.

Denman, K. L., et al. (2007), Couplings between changes in the climate system and biogeochemistry, in *Climate Change 2007: The Physical Science Basis. Contribution of Working Group I to the Fourth Assessment Report of the Intergovernmental Panel on Climate Change*, edited by S. Solomon, pp. 501–568, Cambridge Univ. Press, Cambridge, U. K.

Dickson, A. G. (1990), Thermodynamics of the dissociation of boric acid in synthetic seawater from 273.15 to 318.15K, *Deep Sea Res., Part A*, *37*(5), 755–766.

Dickson, A. G., and F. J. Millero (1987), A comparison of the equilibrium-constants for the dissociation of carbonic-acid in seawater media, *Deep Sea Res., Part A*, *34*(10), 1733–1743.

Dong, S., J. Sprintall, S. T. Gille, and L. Talley (2008), Southern Ocean mixed-layer depth from Argo float profiles, *J. Geophys. Res.*, *113*, C06013, doi:10.1029/2006JC004051.

Friedlingstein, P., et al. (2006), Climate-carbon cycle feedback analysis: Results from the (CMIP)-M-4 model intercomparison, *J. Clim.*, *19*(14), 3337–3353, doi:10.1175/JCLI3800.1.

Gruber, N., et al. (2009), Oceanic sources, sinks, and transport of atmospheric CO_2, *Global Biogeochem. Cycles*, *23*, GB1005, doi:10.1029/2008GB003349.

Hanawa, K., and L. D. Talley (2001) Mode waters, in *Ocean Circulation and Climate*, *Int. Geophys. Ser.*, vol. 77, edited by G. Siedler, J. A. Church, and J. Gould, pp. 373–386, Acad. Press, San Diego, Calif.

Ho, D. T., C. S. Law, M. J. Smith, P. Schlosser, M. Harvey, and P. Hill (2006), Measurements of air-sea gas exchange at high wind speeds in the Southern Ocean: Implications for global parameterization, *Geophys. Res. Lett.*, *33*, L16611, doi:10.1029/2006GL026817.

Hood, E. M., and L. Merlivat (2001), Annual to interannual variations of fCO_2 in the northwestern Mediterranean Sea: Results from hourly measurements made by CARIOCA buoys, 1995–1997, *J. Mar. Res.*, *59*(1), 113–131, doi:10.1357/002224001321237399.

IPCC (2007), *Climate Change 2007: The Physical Science Basis. Contribution of Working Group I to the Fourth Assessment Report of the Intergovernmental Panel on Climate Change*, edited by S. Solomon et al., 996 pp., Cambridge Univ. Press, Cambridge, U. K.

Keeling, C. D., T. P. Whorf, M. Wahlen, and J. Vanderplicht (1995), Interannual extremes in the rate of rise of atmospheric carbon-dioxide since 1980, *Nature*, *375*(6533), 666–670, doi:10.1038/375666a0.

Lee, K., L. T. Tong, F. J. Millero, C. L. Sabine, A. G. Dickson, C. Goyet, G. H. Park, R. Wanninkhof, R. A. Feely, and R. M. Key (2006), Global relationships of total alkalinity with salinity and temperature in surface waters of the world's oceans, *Geophys. Res. Lett.*, *33*, L19605, doi:10.1029/2006GL027207.

Le Quéré, C., T. Takahashi, E. T. Buitenhuis, C. Rödenbeck, and S. C. Sutherland (2010), Impact of climate change on the global oceanic sink of CO_2, *Global Biogeochem. Cycles*, *24*, GB4007, doi:10.1029/2009GB003599.

Letelier, J., O. Pizarro, and S. Nuñez (2009), Seasonal variability of coastal upwelling and the upwelling front off central Chile, *J. Geophys. Res.*, *114*, C12009, doi:10.1029/2008JC005171.

Leth, O., G. Shaffer, and O. Ulloa (2004), Hydrography of the eastern South Pacific Ocean: Results from the Sonne 102 cruise, May–June

1995, *Deep Sea Res., Part II*, *51*(20–21), 2349–2369, doi:10.1016/j.dsr2.2004.08.009.

Locarnini, R. A., A. V. Mishonov, J. I. Antonov, T. P. Boyer, and H. E. Garcia (2006), *World Ocean Atlas 2005*, vol. 1, *Temperature*, *NOAA Atlas NESDIS 61*, edited by S. Levitus, 182 pp., U.S. Govt. Print. Off., Washington, D. C.

Lovenduski, N. S., N. Gruber, S. C. Doney, and I. D. Lima (2007), Enhanced CO_2 outgassing in the Southern Ocean from a positive phase of the Southern Annular Mode, *Global Biogeochem. Cycles*, *21*, GB2026, doi:10.1029/2006GB002900.

McCartney, M. S. (1977) Subantarctic Mode Water, in *A Voyage of Discovery*, George Deacon 70th anniversary volume, edited by M. Angel, pp. 103–119, Pergamon Press, Oxford, U. K.

McNeil, B. I., N. Metzl, R. M. Key, R. J. Matear, and A. Corbiere (2007), An empirical estimate of the Southern Ocean air-sea CO_2 flux, *Global Biogeochem. Cycles*, *21*, GB3011, doi:10.1029/2007GB002991.

Mehrbach, C., C. H. Culberson, J. E. Hawley, and R. M. Pytkowicz (1973), Measurement of the apparent dissociation constants of carbonic acid in seawater at atmospheric pressure, *Limnol. Oceanogr.*, *18*(6), 897–907, doi:10.4319/lo.1973.18.6.0897.

Merlivat, L., M. G. Davila, G. Caniaux, J. Boutin, and G. Reverdin (2009), Mesoscale and diel to monthly variability of CO_2 and carbon fluxes at the ocean surface in the northeastern Atlantic, *J. Geophys. Res.*, *114*, C03010, doi:10.1029/2007JC004657.

Metzl, N., B. Tilbrook, and A. Poisson (1999), The annual fCO_2 cycle and the air-sea CO_2 flux in the sub-Antarctic Ocean, *Tellus, Ser. B*, *51*(4), 849–861, doi:10.1034/j.1600-0889.1999.t01-3-00008.x.

Newberger, T. (2004), Palmer 2004 pCO2 system users manual. (Available at http:www.ldeo.columbia.edu/res/pi/CO2/carbondioxide/text/Palmer_PCO2_man_1_2.pdf)

Orsi, A. H., T. Whitworth, and W. D. Nowlin (1995), On the meridional extent and fronts of the Antarctic circumpolar current, *Deep Sea Res., Part I*, *42*(5), 641–673, doi:10.1016/0967-0637(95)00021-W.

Rangama, Y., J. Boutin, J. Etcheto, L. Merlivat, T. Takahashi, B. Delille, M. Frankignoulle, and D. C. E. Bakker (2005), Variability of the net air-sea CO_2 flux inferred from shipboard and satellite measurements in the Southern Ocean south of Tasmania and New Zealand, *J. Geophys. Res.*, *110*, C09005, doi:10.1029/2004JC002619.

Sabine, C. L., et al. (2004), The oceanic sink for anthropogenic CO_2, *Science*, *305*, 367–371, doi:10.1126/science.1097403.

Saenko, O. A., A. J. Weaver, and M. H. England (2003), A region of enhanced northward Antarctic Intermediate Water transport in a coupled climate model, *J. Phys. Oceanogr.*, *33*(7), 1528–1535, doi:10.1175/1520-0485(2003)033<1528:AROENA>2.0.CO;2.

Sallée, J. B., R. Morrow, and K. Speer (2008), Eddy heat diffusion and Subantarctic Mode Water formation, *Geophys. Res. Lett.*, *35*, L05607, doi:10.1029/2007GL032827.

Sallée, J. B., K. G. Speer, and S. R. Rintoul (2010), Zonally asymmetric response of the Southern Ocean mixed-layer depth to the Southern Annular Mode, *Nat. Geosci.*, *3*, 273–279, doi:10.1038/ngeo812.

Sweeney, C., E. Gloor, A. R. Jacobson, R. M. Key, G. McKinley, J. L. Sarmiento, and R. Wanninkhof (2007), Constraining global air-sea gas exchange for CO_2 with recent bomb C-14 measurements, *Global Biogeochem. Cycles*, *21*, GB2015, doi:10.1029/2006GB002784.

Takahashi, T., et al. (2002), Global sea-air CO_2 flux based on climatological surface ocean pCO(2), and seasonal biological and temperature effects, *Deep Sea Res., Part II*, *49*(9–10), 1601–1622, doi:10.1016/S0967-0645(02)00003-6.

Takahashi, T., et al. (2009a), Climatological mean and decadal change in surface ocean pCO(2), and net sea-air CO_2 flux over the global oceans, *Deep Sea Res., Part II*, *56*(8–10), 554–577, doi:10.1016/j.dsr2.2008.12.009.

Takahashi, T., S. C. Sutherland, and A. Kozyr (2009b), Global ocean surface water partial pressure of CO_2 database: Measurements performed during 1968–2008 (version 2008), *ORNL/CDIAC-152, NDP-088r*, Carbon Dioxide Inf. Anal. Cent., Oak Ridge Natl. Lab., U.S. Dept. of Energy, Oak Ridge, Tenn., doi:10.3334/CDIAC/otg.ndp088r.

Talley, L. D. (1999), Some aspects of ocean heat transport by the shallow, intermediate and deep overturning circulations, in *Mechanisms of Global Climate Change at Millennial Time Scales*, *Geophys. Monogr. Ser.*, vol. 112, pp. 1–22, AGU, Washington, D. C.

Tsuchiya, M., and L. D. Talley (1998), A Pacific hydrographic section at 88°W: Water-property distribution, *J. Geophys. Res.*, *103*(C6), 12,899–12,918, doi:10.1029/97JC03415.

Wanninkhof, R. (1992), Relationship between wind-speed and gas-exchange over the ocean, *J. Geophys. Res.*, *97*(C5), 7373–7382, doi:10.1029/92JC00188.

Wanninkhof, R., W. E. Asher, D. T. Ho, C. Sweeney, and W. R. McGillis (2009), Advances in quantifying air-sea gas exchange and environmental forcing, *Annu. Rev. Mar. Sci.*, *1*, 213–244, doi:10.1146/annurev.marine.010908.163742.

Weiss, R. F. (1974), Carbon dioxide in water and seawater: The solubility of a non-ideal gas, *Mar. Chem.*, *2*, 203–215, doi:10.1016/0304-4203(74)90015-2.

L. Barbero, J. Boutin, N. Martin, and L. Merlivat, LOCEAN, IPSL, CNRS, IRD, UPMC, Case 100, 4 pl. Jussieu, F-75252 Paris, France.

S. C. Sutherland and T. Takahashi, Lamont-Doherty Earth Observatory, Columbia University, 61 Rte. 9W, PO Box 1000, Palisades, NY 10964-1000, USA.

R. Wanninkhof, Atlantic Oceanographic and Meteorological Laboratory, NOAA, 4301 Rickenbacker Causeway, Miami, FL 33149, USA.